SUPPRESSION OF STIMULATED BRILLOUIN SCATTERING BY MODE COUPLING INDUCED WITH SEEDED ION WAVES

B. I. Cohen *A. B. Langdon*

H. A. Baldis *B. F. Lasinski*

E. A. Williams *C. Labaune**

Introduction

Results from recent laser-plasma experiments conducted at the Laboratoire pour L'Utilisation des Lasers Intenses (LULI)[1] have direct relevance to our laser fusion research and to proposed experiments at the National Ignition Facility (NIF). The LULI researchers observed that the primary ion-acoustic wave (IAW) produced by stimulated Brillouin backscattering (SBBS) of one pump laser beam could be substantially reduced in amplitude in the presence of a secondary SBBS process. The secondary process involved a seed laser beam propagating at a relative angle of 22.5°.

The LULI observation and its elucidation are of significant interest for several reasons. First, the study and control of SBBS have been the object of ongoing theoretical and experimental research for many years because of the importance of SBBS in laser fusion.[2–13] The symmetric compression of fusion targets in either direct drive or indirect drive can be affected by SBBS and other parametric instabilities unless such instabilities are controlled. Second, the NIF will have multiple crossing laser beams and require careful control over the timing and relative amplitudes of the crossing beams.[14] To optimize the fusion performance of experiments proposed for the NIF, the interaction of simultaneous SBBS events in crossing laser beams should be understood. Finally, the nonlinear interaction of driven waves in a plasma is of fundamental interest.

Using model simulations and a mode-coupling analysis, we propose a mechanism that can explain some of the LULI observations. Our research makes use of the BZOHAR, 2D, hybrid (particle ions and Boltzmann fluid electrons) simulation code. The BZOHAR code was introduced and described in more detail in Cohen et al.[15] In brief, Poisson's equation with a nonlinear Boltzmann electron response is solved in two spatial dimensions for the self-consistent, scalar electric potential with the ion density collected from particle ion positions. The Maxwell curl equations are reduced via a temporal envelope approximation to a Schroedinger-like equation for the high-frequency, transverse-wave amplitude. The electron ponderomotive potential arising from the transverse waves is included in the electron Boltzmann response.

Our simulations and analysis indicate that mode coupling of ion waves in the primary and secondary SBBS processes leads to enhanced damping of ion waves. Such mode coupling reduces the ion-wave amplitudes and SBBS reflectivities, as observed in the LULI experiments. Our work is also a logical extension of the earlier work of Maximov et al., which addressed the effects of long-wavelength velocity and density perturbations in detuning stimulated Brillouin scattering (SBS).[16]

Simulations and Analysis

Figures 1 and 2 show the results of 2D, doubly periodic, electrostatic simulations of ponderomotively driven ion waves. The results in Figure 1 are from three simulations in which a primary IAW was resonantly excited by an imposed electron ponderomotive potential. In these simulations, the driver amplitude $e\phi_0 / T_e = 0.05$, $k_s\lambda_{De} = 0.1$ for the driven wave, and $T_e / T_i = 10.27$ in a CH plasma, where the plasma parameters were motivated by the LULI experiments. Here, k_s is the wave number of the driven acoustic wave, λ_{De} is the electron Debye length, and T_e and T_i are the electron and ion temperatures, respectively.

In the first simulation, shown on the left in Figure 1, there was no seeded secondary IAW. The primary IAW relaxed via a decay instability[15] after being driven to a large amplitude. In the second and third simulations shown in Figure 1, a secondary IAW was excited at nearly the same frequency, but at a relative angle of 18°

*Laboratoire pour L'Utilisation des Lasers Intenses, Centre National de la Recherche Scientifique, Cedex, France

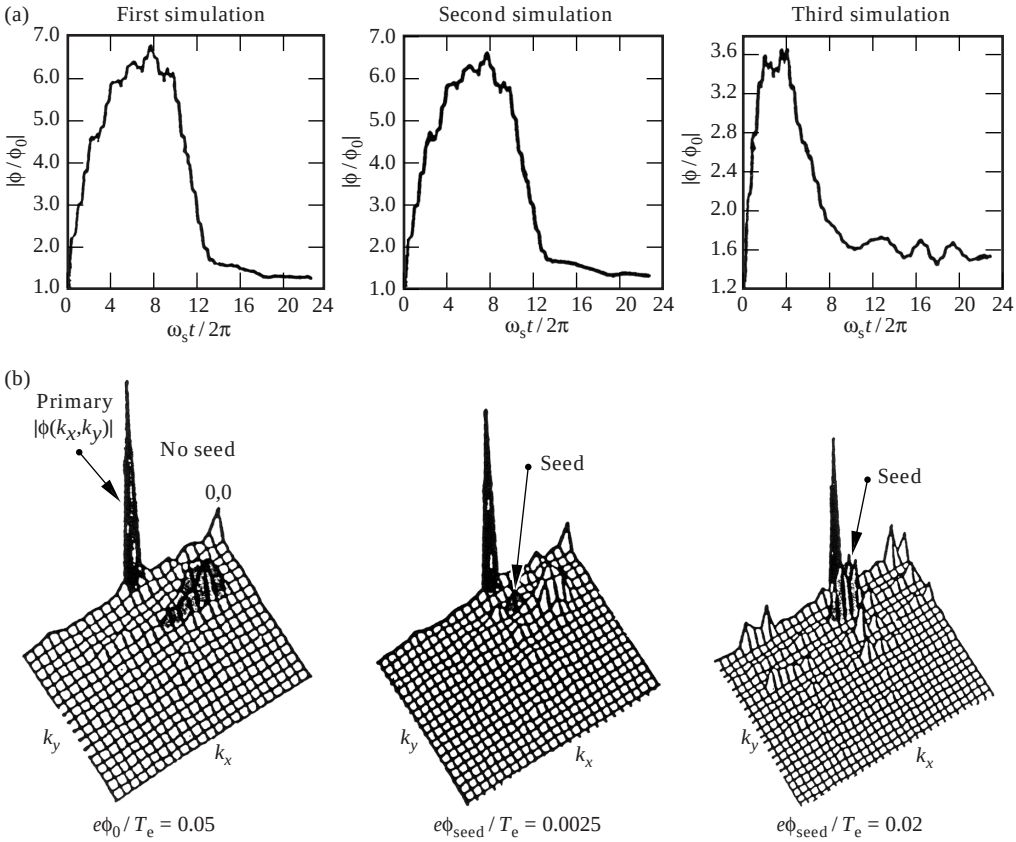

FIGURE 1. (a) Ratio of Fourier amplitudes at the driving frequency and wave number of the plasma electric potential and electron ponderomotive potential $|\phi/\phi_0|$ as a function of time for $e\phi_0/T_e = 0.05$. No seeded secondary IAW was used in the first simulation. In the second simulation, $e\phi_{seed}/T_e = 0.0025$. In the third simulation, $e\phi_{seed}/T_e = 0.02$. (b) The corresponding $|\phi(k_x, k_y)|$ versus k_x and k_y at $\omega_s t/2\pi = 12$ with a $128\Delta x \times 128\Delta y$ domain, 64 particles per species per cell, $k_s\lambda_{De} = 0.1$ for the driven wave, and acoustic driving frequency $\omega_s = k_s c_s/(1 + k_s^2\lambda_{De}^2)^{1/2}$, where c_s is the sound speed, and the seed wave is at an angle of 18° with respect to the primary laser beam.
(50-00-0898-1681pb01)

and with driver amplitudes $e\phi_{seed}/T_e = 0.0025$ and 0.02, respectively. The primary and secondary wave-driving amplitudes were turned on smoothly over two acoustic periods and then left on. The collapse of the primary IAW in the first simulation is caused by the parametric decay into two ion waves at the half-harmonic of the primary IAW k_x wave number and with finite, but generally smaller, k_y. The two-ion-wave parametric decay has been described in Ref. 15 and elsewhere.[17] The primary ion-wave response to its driving potential as a function of time was only minimally reduced by secondary seeding with $e\phi_{seed}/T_e = 0.0025$. However, the primary IAW was reduced substantially for $e\phi_{seed}/T_e = 0.02$, so that the primary IAW did not exceed the threshold for the decay instability.[15] The seed IAW amplitudes were never large enough to exceed this threshold.

Figure 2 shows time histories of the amplitudes of the primary, seed, and beat waves of the primary and seed in the strongly seeded case. The beats of the primary and strong seed grew at the expense of the primary and the seed, and all of the modes ultimately were damped by heating the ions. The decay modes of the primary IAW were observed to grow to amplitudes of $|e\phi/T_e| \approx 0.05$ for the weakly driven seed. In the strongly seeded case, however, the decay modes of the primary IAW achieved amplitudes of $|e\phi_k/T_e| \leq 2 \times 10^{-3}$, which were typical of the simulation noise level in these driven plasmas. The amplitudes of the second and third harmonics of the primary wave tracked the growth and relaxation of the primary in this strongly seeded case. Significant ion trapping and acceleration of a fast ion tail resulted from the action of the primary wave.[5,7,15]

For the simulations shown in Figure 1, the peak amplitudes of the primary ion-wave were $|e\phi_k/T_e| \approx 0.15$ to 0.3. The amplitudes then relaxed to $|e\phi_k/T_e| \approx 0.05$ on a time scale of 5 to 10 acoustic periods. The relaxation is due to the action of ion-wave parametric decay or mode coupling and damping on the ion velocity distribution function. This relatively fast time scale is shorter than the 50-ps temporal resolution of the Thomson scattering used to diagnose the ion-wave amplitudes in the LULI experiments. The LULI measurements suggested ion-wave amplitudes no larger than $|\delta n_e/n_0| \approx |e\phi/T_e| \approx 0.1$. The strength of the mode coupling depends on the product of the primary and secondary IAW amplitudes. With $|e\phi_0/T_e| = 0.01$, which led with no secondary seeding to a peak response $|\delta n_e/n_0| \approx 0.1$, as in the LULI observations, and seeding with $e\phi_{seed}/T_e = 0.003$, we observed in our simulation a peak primary wave amplitude $|\delta n_e/n_0| = 0.08$. This value represents a 20% reduction due to mode coupling with the seed IAW.

Our electrostatic simulations show that mode coupling with the seed IAW provides an additional loss

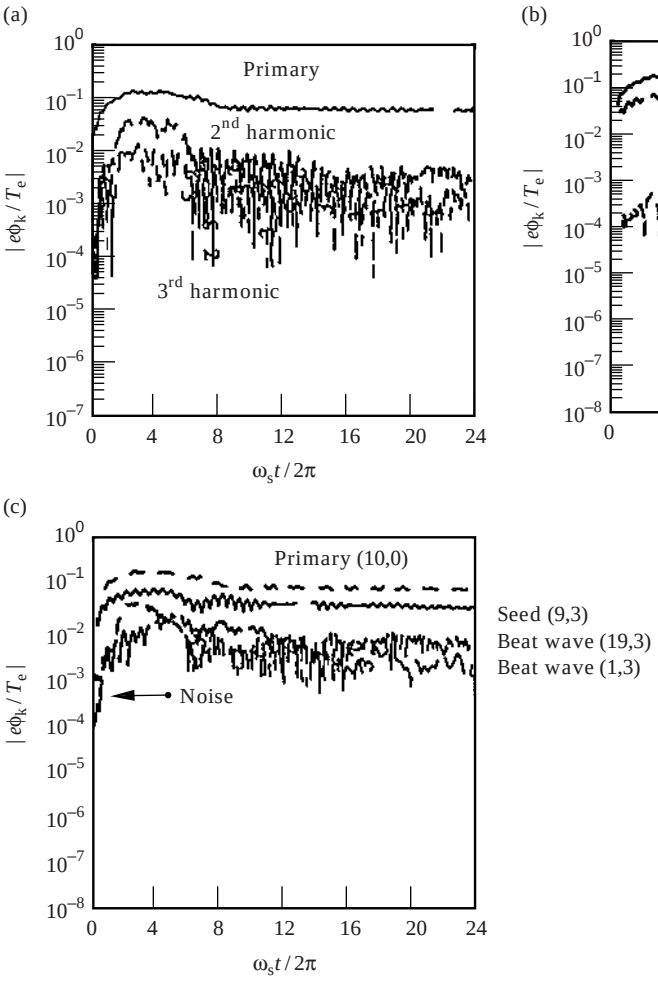

FIGURE 2. Time histories of amplitudes $|e\phi_k / T_e|$ of (a) the primary IAW and its second and third harmonics, (b) the seed wave and a decay mode of the primary, and (c) the beats of the seed and primary IAW for the strongly seeded case in Figure 1. The number pairs in parentheses indicate the *x* and *y* mode numbers of the waves.
(50-00-0898-1682pb01)

channel for the primary IAW, and for the seed as well. The following mode-coupling analysis illustrates how the coupling of ion waves leads to additional dissipation for the primary IAW that reduces its amplification by SBBS and reduces the SBBS reflectivity. Consider the following simplified set of coupled-mode equations for modeling resonant SBBS and heavily damped ion waves in a uniform plasma in steady state:

$$-v_g \frac{\partial a_1}{\partial x} = c_1 a_0^* a_{s1} \tag{1a}$$

for a backscattered transverse wave,

$$\frac{da_{s1}}{dt} = c_2 a_0 a_1 - \gamma_{s1} a_{s1} - c_3 a_{s2} a_{s3} = 0 \tag{1b}$$

for a primary IAW, and

$$\frac{da_{s3}}{dt} = c_4 a_{s1} a_{s2}^* - (\gamma_{s3} + i\Delta_{s3}) a_{s3} = 0 \tag{1c}$$

for a beat-wave IAW.

Here,

- c_1, c_2, c_3, and c_4 are coupling coefficients that can be identified in the analyses of SBBS [2–4,6,7] and the two-ion-wave parametric decay.[15]
- v_g is the group velocity of the backscattered electromagnetic wave.
- *da/dt* is a convective time derivative on a wave amplitude *a*.
- γ_{s1} and γ_{s2} are linear dissipation rates for the ion waves.
- a_0 and a_1 are the amplitudes of the pump and backscattered electromagnetic waves.
- a_{s1}, a_{s2}, and a_{s3} are the ion-wave amplitudes for the primary, seed, and beat waves.
- Δ_{s3} is a frequency mismatch.

The mode-coupling equations are readily solved in steady state when the seed amplitude a_{s2} is a fixed parameter. From Eqs. 1b and 1c,

$$a_{s3} = \frac{c_4 a_{s1} a_{s2}^*}{\gamma_{s3} + i\Delta_{s3}} , \tag{2a}$$

and

$$a_{s1} = \frac{c_2 a_0 a_1}{\gamma_{s1}^{nl}} \ , \tag{2b}$$

where Re γ_{s1}^{nl} is the effective damping of the primary IAW, and

$$\gamma_{s1}^{nl} = \gamma_{s1} + \frac{c_3 c_4 |a_{s2}|^2}{\gamma_{s3} + i\Delta_{s3}} \ . \tag{3}$$

The second term in Eq. 3 represents the enhancement of the damping of the primary IAW arising from mode coupling induced by the seed. A spatial growth rate for SBBS is obtained from Eqs. 1a and 2, as follows:

$$\kappa = -\frac{\partial \ln(a_1)}{\partial x} = \frac{c_1 c_2 |a_0|^2}{v_g \gamma_{s1}^{nl}} = \frac{\gamma_{SBS}^2}{v_g \gamma_{s1}^{nl}} \ , \tag{4}$$

where γ_{SBS} is the homogeneous-medium temporal growth rate for weakly coupled Brillouin backscatter.[2–4,6,7] The exponential amplification of both the backscattered electromagnetic wave amplitude and the primary IAW amplitude in the backward direction over a length L is given by κL. The gain exponent $G \equiv \kappa L$ has been altered by the mode coupling induced by the seed IAW from the gain exponent in the absence of the seed, $G_0 \equiv \gamma_{SBS}{}^2 L / v_g \gamma_{s1}$:

$$G = \frac{\gamma_{s1}}{\gamma_{s1}^{nl}} G_0 \ . \tag{5}$$

The mode coupling leads to enhanced damping of the primary ion wave if $|\gamma_{s1}{}^{nl}/\gamma_{s1}| > 1$, and the gain exponent is reduced correspondingly. A 20% enhancement of the effective dissipation is suggested by the 20% reduction of the primary IAW from our ponderomotively driven electrostatic simulations using parameters appropriate to the LULI experiment. Then, for $G_0 = 5$, which is a typical value for the LULI experiment with laser intensity $I_0 = 10^{14}$ W / cm^2 (Ref. 18), the square of the relative density perturbation in the primary IAW is expected to be reduced by $[\exp(-5 \times 0.2)]^2 = 0.14$. This estimate is in rough agreement with the LULI observations.[1]

If the seed IAW leads to enhanced damping of the primary IAW via mode coupling, we would expect a similar effect on the seed because of the action of the primary IAW. This result is observed in the time histories in Figure 2. After the primary and seed IAW amplitudes are driven to finite amplitudes, they both decay accompanying and following the growth of the beat waves of the seed and primary IAWs. This effect can be understood by augmenting the coupled-mode equations, Eqs. 1a, 1b, and 1c, to include a dynamical equation for the seed IAW of the same form as Eq. 1b. The seed IAW then acquires an enhanced damping rate arising from the mode coupling induced by the primary and the seed of the same form as that in Eq. 3.

The seed IAW in the LULI experiments is excited by the interaction of a seed laser beam propagating at a finite relative angle with respect to the primary laser beam. In our simulations, we considered only the effects of a single, specific seed IAW with the backscatter IAW of the primary laser beam. Dubois, Bezzerides, and Rose[19] analyzed the collective parametric instabilities of many overlapping and converging laser beams. Their formulation is a useful reference for understanding the following qualitative arguments. The Thomson scattering diagnostics in the LULI experiments reveal that, for a weak seed laser strength, the backscatter IAW is the dominant IAW.[1] Therefore, we focused on the mode coupling of the backscatter IAWs of both the primary and the secondary laser beams in this work. However, in the LULI experiments, there was also the mutually resonant IAW propagating at an angle that bisected the angle between the propagation directions of the two laser beams. This mutually resonant IAW was jointly driven by the SBS ponderomotive forces of the primary and seed laser beam. Thus, it was not surprising that its amplitude was enhanced as the seed laser strength was increased. The square of the mutually resonant IAW amplitude scaled approximately linearly with seed laser intensity, suggesting that the seed and primary SBS ponderomotive forces added incoherently.[19] Figures 2, 3, and 4 of Ref. 1 indicate that the primary backscatter IAW amplitude for zero seed laser intensity was larger over a greater volume than was the amplitude of the mutually resonant IAW, which was enhanced over only a very narrow cone of angles. In addition, the suppression effect of the backscatter IAW was more dramatic than was the enhancement effect of the mutually resonant IAW. The overall reflectivities in the LULI experiment were relatively low, ~5%. Pump depletion was not believed to be significant, except perhaps over a short-lived, transient time scale that the diagnostics could not resolve in the experiments.[18]

Our simulations considered only a single seed and primary IAW, rather than a spectrum of IAWs propagating at various angles. We present quantitative arguments for the efficacy of the seed IAW associated with the backscatter of the seed laser in suppressing the backscatter of the primary laser via mode coupling of the IAWs. We expect that the mutually resonant IAW also mode couples with the primary IAW and aids in the suppression effect, because the physics of the mode coupling with the primary IAW is qualitatively the same for both the mutually resonant and nonresonant seed IAWs. Thus, our model calculations likely underestimate the suppression effects of mode coupling on the backscatter of the primary by omitting the mutually resonant IAW. The inclusion of the mutually

resonant IAW in our simulations and a quantitative analysis are beyond the scope of this paper and will be the subject of future research.

To corroborate the suppression of SBBS by mode coupling induced with a seed IAW, we performed electromagnetic simulations of SBBS with a ponderomotively driven, plane-wave seed IAW propagating at 30° with respect to the primary IAW excited by SBBS. These simulations allowed only exactly forward and backward scattered electromagnetic waves ($k_y = 0$) with radiative (outgoing-wave) and charge-conserving boundary conditions in x and periodicity in y. The mesh was $2600\Delta x \times 512\Delta y$, with 25 particles per ion species per cell, $\lambda_{De} \approx \Delta x$, $T_e = 0.6$ keV, $T_e / T_i = 2.4$ in a CH plasma, $L_x \approx 42\lambda_0$, and $L_y \approx 8\lambda_0$. Here, λ_0 is the laser wavelength, and $k_s\lambda_{De} = 0.2$.

Figure 3 shows the results of three electromagnetic simulations for $e\phi_{seed} / T_e = \{0.01, 0.07, 0.14\}$ and a plane-wave laser beam corresponding to 10^{14} W / cm^2 at a wavelength of 1 μm. The time histories of the instantaneous and cumulative time-averaged reflectivities, and the amplitudes $(e\phi_k / T_e)^2$ of the primary IAW in each case demonstrated a significant reduction of reflectivities for $t > 20$ ps and of the primary IAW amplitudes as $e\phi_{seed} / T_e$ was increased. We also performed an additional simulation with no seed, $e\phi_{seed} / T_e = 0$. The results for the time histories of backscatter reflectivities and primary IAW amplitudes were the same as those shown in Figure 3a for $e\phi_{seed} / T_e = 0.01$.

These results illustrate that suppression effects of the seed IAW require both finite amplitude and finite time in which to occur. The maximum observed reflectivities and IAW amplitudes for $t < 20$ ps were unaffected by IAW mode coupling, whose effects set in at a later time after the primary and seed IAWs acquired finite amplitudes. This can be understood by retaining time derivatives in Eqs. 1b and 1c and considering the dynamics. The first peak in the reflectivities and the subsequent relaxation were affected by several nonlinearities observed in the simulation diagnostics. The nonlinearities include ion trapping, transient ion-wave harmonic generation, parametric decay of the primary IAW,[15] and partial pump depletion and associated nonlinear oscillations in reflectivity.

The LULI data demonstrated that the reduction of the primary IAW amplitude was directly correlated with the intensity of the seed laser beam driving the

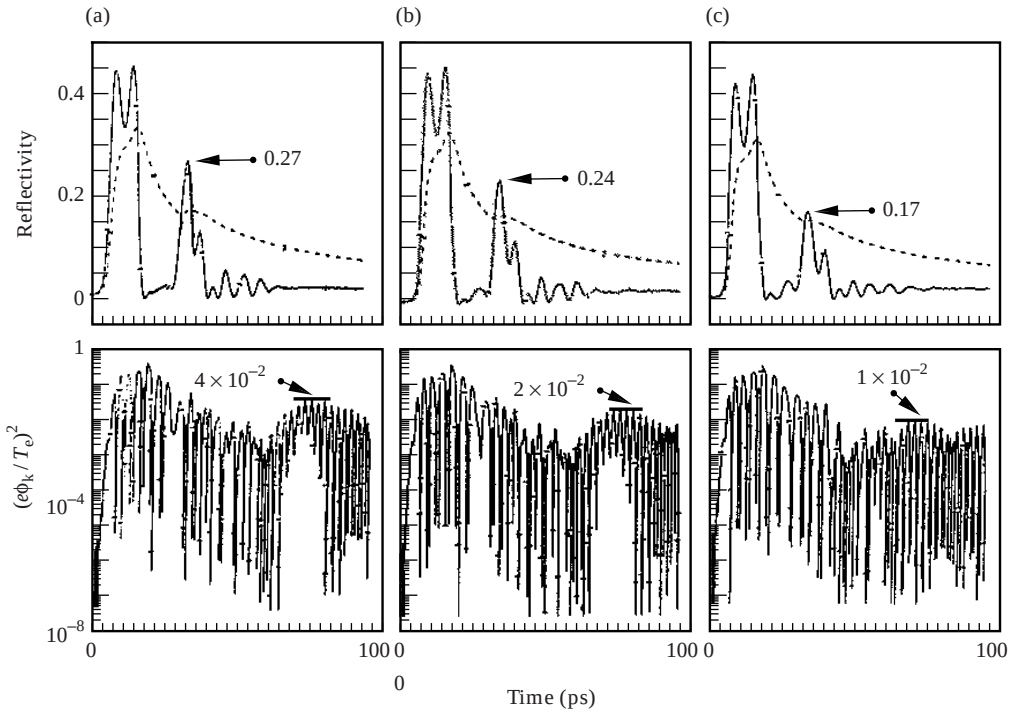

FIGURE 3. Time histories of the instantaneous (solid curve) and cumulative average (dashed curve) reflectivities and primary IAW amplitudes $|e\phi_k / T_e|^2$ as functions of time for (a) $e\phi_{seed} / T_e = 0.01$, (b) $e\phi_{seed} / T_e = 0.07$, and (c) $e\phi_{seed} / T_e = 0.14$. This simulation is in a CH plasma with hydrogen-to-electron mass ratio $m_H / m_e = 1836$, $T_e / T_i = 2.4$, and $k_s\lambda_{De} = 0.2$. The laser electron quiver velocities $v_0^L / v_e = 0.577$ for the input value of the primary laser beam incident from the left side of the simulation. For the input value of the backscatter wave at the right side of the simulation, $v_0^R / v_e = 0.0577$. Here, $v_e = (T_e / m_e)^{1/2}$, and the electron density was equal to 10% critical density. The time histories of $|e\phi_k / T_e|^2$ were computed from the Fourier transform of the electric potential with respect to y at a position $x = L_x / 4$. (50-00-0898-1683pb01)

secondary SBBS process. To more directly connect the results shown in Figure 3 with the LULI data, we performed a series of SBBS simulations with no IAW seeding, but with varying laser intensity. Keep in mind that this is not a self-consistent electromagnetic simulation of the two interacting SBS events, which is beyond the scope of our simulation model. However, mode coupling produced by both the seed and primary IAWs requires a finite time to have a damping effect after the seed and primary IAWs reach finite amplitude. Thus, the relation between the peak SBBS IAW amplitude and single pump laser intensity, and the results of Figure 3, provide a first approximation to the seed laser intensity needed to suppress the backscatter of the primary SBBS.

Figure 4 shows our results for the peak instantaneous reflectivities, the cumulative reflectivities (time-averaged over 100 ps), and peak IAW amplitude $(e\phi_k / T_e)^2$. The results are plotted as functions of the average seed laser intensity I_s / I_0, where $I_0 = 10^{14}$ W/cm^2, with no primary laser beam present. We used the same LULI plasma parameters as in Figure 3. (The seed pump laser was incident from the left side of the simulation box. The input value of the backscattered electromagnetic wave at the right side boundary for the series of simulations shown in Figure 4 was fixed at a relative intensity of 0.005 I_0. The reflectivities and concomitant peak primary IAW amplitudes were relatively insensitive to this input value.) The simulation reflectivity was 5% when averaged over 100 ps for $I_s = I_0$ (the reference LULI intensity). There was also a sharp decrease in reflectivity with decreasing laser intensity. Both of these results are in reasonable agreement with the LULI observations.[18] For $I_s / I_0 < 0.5$, no ion-wave decay instability was observed in our simulations because the peak amplitudes of the primary SBBS IAW were below threshold for the decay instability ($|e\phi_k / T_e| < 0.2$ in this case).[15] When comparing particle simulations of SBBS to experiments, it is important to take into account the temporal resolution of the experimental measurements (typically ≥50 ps). The peak reflectivities and other transient features occurring on time scales less than ~20 ps in the simulations cannot be resolved in the laboratory experiments.

The results from Figure 4 allow us to infer the corresponding seed laser intensity required to produce the seed IAW amplitude used to suppress the primary SBBS process. Figure 5 compares the LULI data on backscatter suppression to our results from the BZOHAR simulation. The primary IAW amplitude $(e\phi_k / T_e)^2$ was reduced to 1/4 its value at the inferred intensity $I_s / I_0 = 0.35$, when compared to its amplitude with no seeding in the simulation. The primary IAW was reduced to 1/6 its unseeded value at an intensity $I_s / I_0 = 0.3$ in the LULI experiments. We expect that by including in our model the other ion waves (including the mutually resonant IAW) produced by the two interacting SBS events, there would be additional mode coupling and a further enhancement of the suppression of the backscatter of the primary pump laser. However, such an inclusion is beyond the scope of our simulation model.

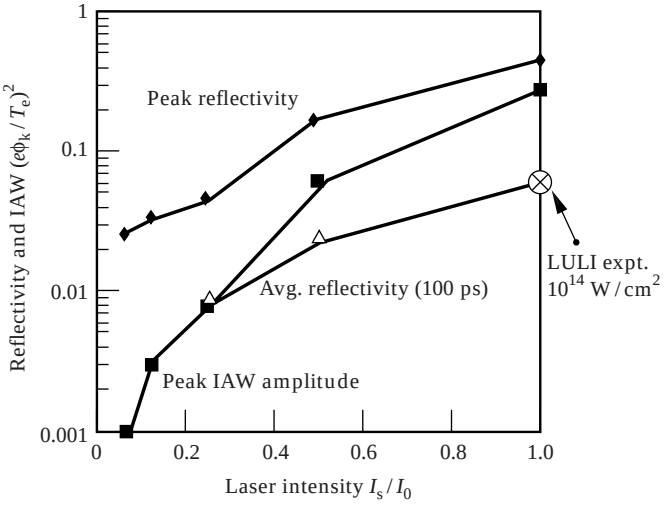

FIGURE 4. Peak and time-averaged (0- to 100-ps, Δ) reflectivities, and peak IAW amplitudes $|e\phi_k / T_e|^2$ as functions of relative seed laser intensity I_s / I_0 for $I_0 = 10^{14}$ W/cm^2. Results are from a series of 2D SBBS backscatter simulations varying v_0^L / v_e incident from the left, and using $v_0^R / v_e = 0.04$ for the backscatter incident from the right. Other parameters were the same as those in Figure 3, with no IAW seeding. (50-00-0898-1684pb01)

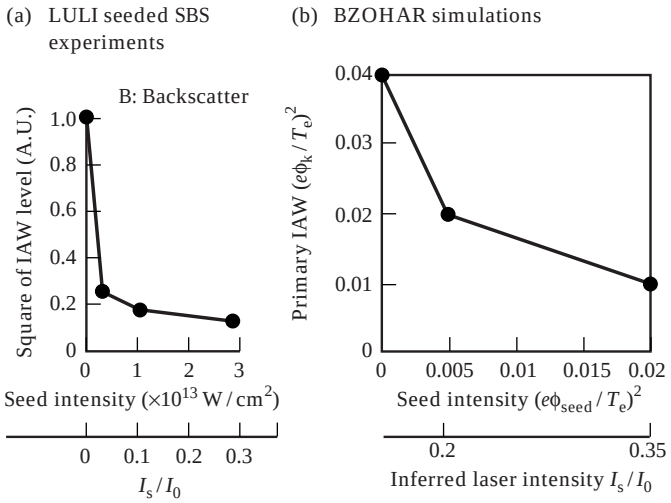

FIGURE 5. (a) Square of the primary SBBS IAW amplitude, in arbitrary units, as a function of seed laser intensity from the LULI experiment.[1] (b) Square of the primary SBBS IAW amplitude $|e\phi_k / T_e|^2$ as a function of seed IAW amplitude and the inferred laser intensity I_s / I_0 from the simulations in Figures 3 and 4. (50-00-0898-1685pb01)

The reflectivities and SBBS suppression exhibited in the simulations are in rough agreement with the LULI observations. Such agreement is somewhat remarkable, given the simplicity of the model. In addition to the omission of the angular spectrum of SBS, the actual laser intensity spatial structure was not incorporated into the simulations. Moreover, the simulation domains were smaller than a single speckle (hot spot) in the LULI beams. However, the simulations did use appropriate, spatially averaged laser intensities and plasma parameters.

The peak reflectivities and corresponding IAW amplitudes may depend on the domain (or speckle) length over which the instability amplifies initially. However, Figure 6 shows the results of an SBBS simulation that suggests that a nonlinear relaxation occurs to a much smaller length scale than the system length, over time scales less than or equal to the temporal resolution of the measurements in the experiments. The picture that emerges from our simulations and multiple-speckle fluid simulations[8] is that SBBS occurs as brief scintillations, dominantly in laser hot spots. Such scintillations give rise to bursts of reflectivity and large-amplitude ion waves. The spatial domains of activity may rapidly shrink as the ion waves and concomitant reflectivity relax with momentum and energy going from the laser to the ion waves, and ultimately into the ion velocity distribution function. The experimental diagnostics integrate in space and time over multiple SBBS scintillations.[18]

Summary

The simulations and analysis presented in this report indicate that a seeded ion wave can induce mode coupling of the seeded and SBBS ion waves (where the seed, SBBS, and beat ion waves are damped on the plasma). Such induced mode coupling substantially suppresses the SBBS reflectivity and its accompanying ion wave. These simulation results are in qualitative agreement with experimental observations by LULI researchers.[1] Such a mechanism may mitigate SBBS activity in other experiments in which intense laser beams cross at finite angles.

Acknowledgments

We are grateful to Richard Berger and other members of the scientific staff at Lawrence Livermore National Laboratory for useful discussions, insight, and encouragement. We also thank the technical groups at LULI for their support.

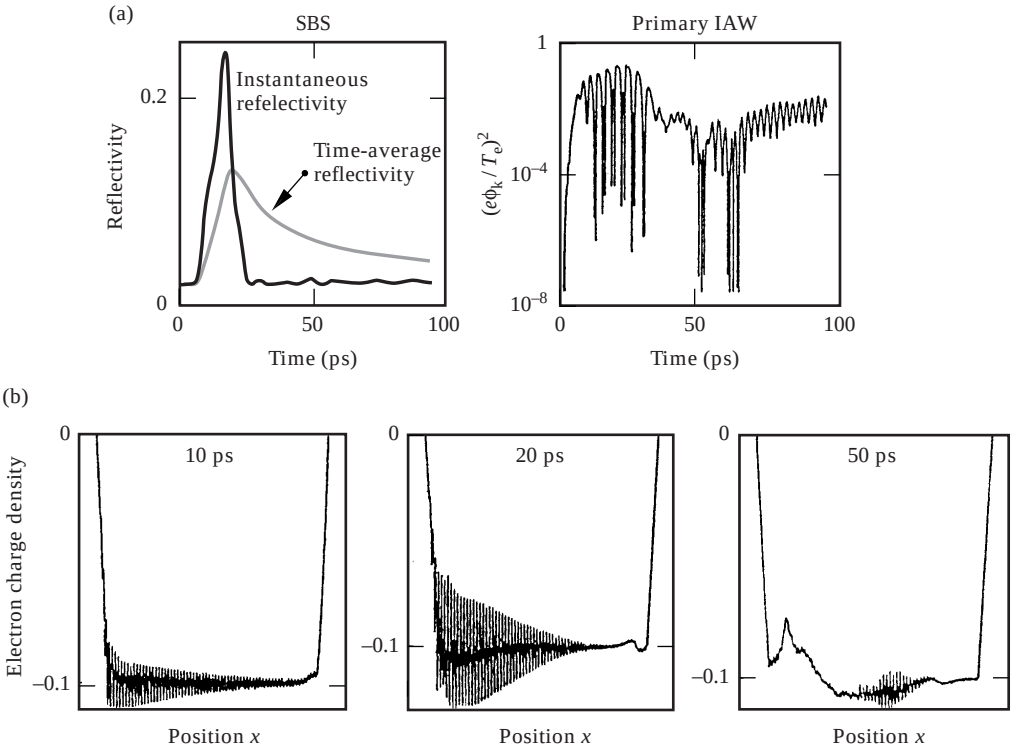

FIGURE 6. (a) Instantaneous and cumulative time-averaged reflectivities, and primary SBBS IAW amplitude $|e\phi_k / T_e|^2$. Results were computed from the Fourier transform of the electric potential with respect to y at $x = L_x / 4$ as functions of time. (b) Snapshots of the y-averaged electron charge density as a function of position x plotted over the entire x domain at 10, 20, and 50 ps. These results are from a simulation with backscatter input boundary condition $v_0^R / v_e = 0.0115$ and no IAW seeding. Other parameters were the same as those in Figure 3.
(50-00-0898-1686pb01)

Notes and References

1. H. A. Baldis, C. Labaune, E. Schifano, N. Renard, and A. Michard, *Phys. Rev. Lett.* **77**, 2957 (1996).
2. V. P. Silin, *Sov. Phys. JETP* **21**, 1127 (1965).
3. J. F. Drake, P. K. Kaw, Y. C. Lee, G. Schmidt, C. S. Liu, and M. N. Rosenbluth, *Phys. Fluids* **17**, 778 (1974).
4. D. W. Forslund, J. M. Kindel, and E. L. Lindman, *Phys. Fluids* **18**, 1002 (1975).
5. D. W. Forslund, J. M. Kindel, and E. L. Lindman, *Phys. Fluids* **18**, 1017 (1975).
6. B. I. Cohen and C. E. Max, *Phys. Fluids* **22**, 1115 (1979).
7. W. L. Kruer, *The Physics of Laser Plasma Interactions* (Addison-Wesley, Reading, MA, 1988).
8. R. L. Berger, B. F. Lasinski, A. B. Langdon, T. B. Kaiser, et al., *Phys. Rev. Lett.* **75**, 1078 (1995).
9. H. A. Baldis, D. M. Villeneuve, C. Labaune, D. Pesme, et al., *Phys. Fluids B* **3**, 2341 (1991).
10. H. A. Baldis, E. M. Campbell, and W. L. Kruer in *Handbook of Plasma Physics*, Vol. 3, A. Rubenchik, ed. (North Holland, Amsterdam, 1990).
11. H. A. Baldis, J. D. Moody, D. S. Montgomery, C. Labaune, et al., *Plasma Phys. Control. Nuc. Fusion Res.* **3**, 221 (1992).
12. L. V. Powers, R. L. Berger, R. L. Kaufman, B. J. MacGowan, et al., *Phys. Plasmas* **2**, 2473 (1995).
13. B. J. MacGowan, B. B. Afeyan, C. A. Back, R. L. Berger, et al., *Phys. Plasmas* **3**, 2019 (1996).
14. National Technical Information Service Document Nos. DE95017671-DE95017673 and DE95017676-DE95017700 (J. A. Paisner, E. M. Campbell, and W. J. Hogan, *The National Ignition Facility Project*, UCRL-JC-117397 and UCRL-PROP-117093, May 1994). Copies may be obtained from Nat. Tech. Inf. Service, Springfield, VA 22161.
15. B. I. Cohen, B. F. Lasinski, A. B. Langdon, and E. A. Williams, *Phys. Plasmas* **4**, 956 (1997).
16. A. V. Maximov, W. Rosmus, V. T. Tikhonchuk, D. F. Dubois, H. A. Rose, and A. M. Rubenchik, *Phys. Plasmas* **3**,1689 (1996).
17. J. A. Heikkinen, S. J. Karttunen, and R. R. E. Salomaa, *Phys. Fluids* **27**, 707 (1984).
18. V. T. Tikhonchuk, C. Labaune, and H. A. Baldis, *Phys. Plasmas* **3**, 3777 (1996).
19. D. F. Dubois, B. Bezzerides, and H. A. Rose, *Phys. Plasmas* **4**, 241 (1992).